Reconfigurable Cellular Base Station Antenna Consisting of Parasitic Radiators

Husnain Ali Kayani, *Student Member*, Quentin Gueuning, *Student Member*, Nicolas Goreux, Danielle Vanhoenacker-Janvier, *Senior Member*, Claude Oestges, *Fellow Member*, and Christophe Craeye, *Senior Member*

***Abstract*—A beamshaping technology, based on arrays of parasitic elements, is presented for the modulation of radiation patterns of existing 4G or 5G base station antennas. First, based on the cell's geographic topology and the requirements of different radiation power exposure, and using ray-tracing simulation, the desired antenna radiation patterns are determined and represented with spherical harmonics. Those patterns are implemented in a prototype in the 1800 MHz band using parasitic radiators, loaded with different impedances, to be placed in front of the existing cellular base station antenna. A smaller prototype demonstrates the electronic control of parasitic loads using varactor diodes. The developed prototypes have been tested in the laboratory and the measurements are in a good agreement with the simulation results.**

***Index Terms*—Beamforming, electronically steerable parasitic array radiator (ESPAR) antenna, 5G communication, mutual coupling, reconfigurable antennas.**

I. Introduction

THE proliferation of mobile communication technologies has increased the human exposure to Radio Frequency (RF) radiation. The mostly followed standards for Base Station (BS) radiation are published by the International Commission on Non-Ionizing Radiation Protection (ICNIRP) [1] which are recognized by the World Health Organization (WHO). In a cellular communication, a BS generally overexposes an area in the line of sight of the main beam and underexposes the rest of the area. Therefore, in order to achieve the required throughput in badly covered areas, a higher transmitted power is needed at the base station, which may lead to harmful RF exposure in certain areas. Taking precautionary measures against the potential RF exposure risk without drastic loss of throughput entails many technical and economic challenges. The use of micro cells network (with smaller antennas) can solve this problem but that is not economically viable. Another way to attain those different goals is to adapt the radiation pattern of a base station antenna according to its environment. In this domain the use of parasitic elements appears as an under-exploited degree of freedom, although it can help to attain lower RF exposure levels for the general public without any major economic impact nor significant reduction of throughput. In this paper, parasitic radiators are used in front of the existing base station antennas to modify their radiation patterns, in order to approximately obtain a specific level of field-strength distribution over the coverage area. So, the idea is first to obtain the desired base station radiation pattern, based on propagation simulations in a given area. Then the second step consists of implementing that desired radiation pattern by placing the parasitic radiators with loads in front of the existing base stations.

In [2], the desired (objective) radiation pattern simply consists of an inverse squared cosine function that compensates for the propagation losses for receivers lying within a plane directly below the base station. Moreover, optimization constraints have been added to reduce the interference by limiting the power sent toward nearby cells. In contrast, [3] uses ray-tracing simulations to produce site-specific antenna patterns which enhance the coverage and the delay spread of the channels within a single cell. Hence, the patterns are shaped according to the geometry of the surrounding streets and buildings. However, since they are obtained from the union of a finite number of small sectors in which the field amplitude is assumed constant, the desired patterns can be discontinuous and highly directive. In this paper, we have implemented a method similar to [3], except that the patterns are represented through a small set of spherical vector wave functions and that the optimization variables are their associated expansion coefficients. It ensures that the solutions are physical since they satisfy Maxwell's equations and that they are sufficiently smooth to be used for base station antennas of limited size. In this paper, the maximum electric field strength of 3 V/m (129.5 dBμV/m) is considered at 1800 MHz to compute the desired radiation patterns for the base station.

The next step is to implement the objective radiation patterns by parasitic arrays at the base station. The driven antennas (here the existing base station antennas) and parasitic radiators with loads are collectively referred to as a parasitic array. Parasitic antenna arrays [4] are becoming popular to implement beamforming and beam-shaping in communication applications, such as 5G communication, the Internet of

Manuscript received November 20, 2018; revised June 06, 2019; accepted July 22, 2019. This work was financially supported by "Régions Wallonne et Bruxelloises" through the B-WARE project.

Husnain Ali Kayani, Danielle Vanhoenacker-Janvier, Claude Oestges and Christophe Craeye are with the ICTEAM Institute, Université catholique de Louvain (UCL), Louvain-la-Neuve, Belgium (e-mail: husnain.kayani@uclouvain.be, danielle.vanhoenacker@uclouvain.be, claude.oestges@uclouvain.be, christophe.craeye@uclouvain.be.

Quentin Gueuning is with the Cavendish Laboratory, University of Cambridge, Cambridge, UK (e-mail: quentin.gueuning@hotmail.com). Nicolas Goreux is with the IBA, Ottignies-Louvain-la-Neuve, Belgium (e-mail: nicolas.goreux@hotmail.com).

Things (IoT) [5], MIMO systems [6], WLAN communication [7] etc. It enables to achieve higher data rate while limiting interference, at an acceptable cost. The reason for employing parasitic arrays is that they are much cheaper than conventional phased arrays. In the latter, each antenna requires its separate radio frequency circuitry, i.e. amplifiers, filters, mixers etc. for the control of amplitude and phase in order to form a specific beam. A parasitic array consists of one or few driven (active) antennas, and mostly parasitic radiators. Beamforming and beam-shaping are achieved by varying the loads (impedances) attached directly to the parasitic radiators [4], [6]. In a parasitic array, all antennas are placed in close proximity to each other in order to have a stronger mutual coupling. The impact of mutual coupling on a radiation pattern varies by tuning the variable loads and thus, different radiation patterns can be obtained [4], [6]. Varactor diodes can be used as variable loads, the impedance is tuned by changing the DC bias voltage and therefore, beam scanning and beam shaping can be carried out electronically [6].

Phased array theory cannot be applied directly to the parasitic array since the loads are directly attached to the parasitic radiators, which hence do not benefit from independent signal control. The use of open-circuit patterns in the calculation of total radiation pattern of parasitic array, includes all the effects mutual coupling [8], [9] and does not entail any underlying approximation. Moreover, this approach avoids launching full-wave simulations at each iteration and therefore it is computationally efficient. The hardware required to develop parasitic antenna arrays is not very expensive but it costs computationally to determine the values of loads [8], since a proper modelling of the effects of mutual coupling generally requires full-wave simulation. The relation between the radiation pattern and parasitic loads is non-linear, which makes it difficult to analytically determine the set of loads that produces the desired radiation pattern [6], [8]. Therefore, an efficient optimization algorithm is needed to achieve that goal. Different deterministic [6], stochastic [10], [11] and meta-heuristic [8] algorithms can be used to find the optimized set of loads. The optimization technique described in [9] uses the spatial harmonic decomposition of loads and it provides the optimum solution in a very short time. That is why this technique will be used here.

After computing the parasitic loads, parasitic array needs to be implemented with the existing base station antenna. In [12], only the beam width of the base station antenna is reconfigured by tuning varactor diodes attached to the parasitic elements. Antennas using frequency selective surface (FSS) with reconfigurable patterns have also been proposed [13], [14], in which PIN diodes (ON or OFF) are used for the reconfigurability of a beam. Reconfigurable transmitarrays have also been designed for beamforming applications [15]. In this paper for the first time, to the author's best knowledge the parasitic antenna array has been designed and implemented for the existing base stations (4G or 5G) to carry out beam-forming and beam-shaping, in order to attain a certain RF exposure within a cell. Here, prototypes have been fabricated consisting of parasitic radiators and loads in front of the base station antenna, operating at 1800 MHz, to accommodate with the higher frequency band of existing base station antennas. Varactor diodes have been used in a smaller prototype to test the electronic reconfigurability.

The remainder of the paper is organized as follows: Section II describes the overall methodology that has been employed in this paper. Section III explains the procedure to compute the objective radiation patterns for base stations by using the propagation tools. Section IV describes the design procedure of the parasitic array and presents the simulation and experimental results. Section V details the design of the electronically steerable parasitic array and its simulation and experimental results. In Section VI, propagation simulation results are shown to verify that coverage has been improved with the required RF power exposure. The conclusions are drawn in Section VII.

II. Methodology

The methodology employed in this paper is illustrated by the flow chart shown in Fig. 1. The addressed optimization problem has been divided into two parts. The ray tracing simulations have been carried out for the given geometry of the cell, using an in-house code. Then the first optimization has been carried out to obtain the objective radiation patterns of the base station antennas, considering the power constraints. The second optimization problem entails the computation of loads of the parasitic array to form the objective radiation patterns, from the existing 4G or 5G base station antennas. An in-house code for the method-of-moments (MoM) has been used for the antenna simulation and then second optimization process is carried out. In the end, the design of the parasitic array is obtained. This whole process improves the coverage of the cell, by modulating the radiation pattern.

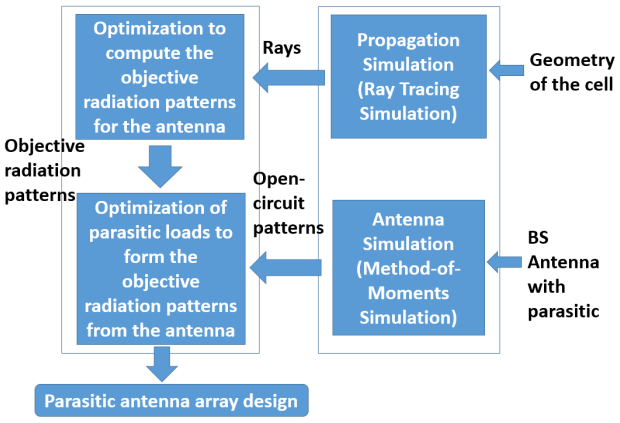

Fig. 1. Flow chart illustrating the proposed methodology.

III. Objective Radiation Patterns

In this section, we will present the formulation of an optimization problem, based on ray-tracing simulations, which will be solved numerically in order to find the desired (objective) pattern. The objective pattern is the one that allows to keep the field level below a certain threshold value in a cell while optimizing the throughput. Later, this pattern will be

used as an objective function to determine the loads of the parasitic array.

Firstly, let us assume that the three-dimensional objective pattern of the antenna can be decomposed into

$$\mathbf{f}_{obj}(\theta,\phi) = \sum_{n=1}^{2(N+1)^2-2} x_n \ \mathbf{f}_n(\theta,\phi) \tag{1}$$

where x_n are unknown expansion coefficients and $\mathbf{f}_n$ are the vector spherical wave functions [16]. Its radiated power is given by:

$$P = \frac{\mathbf{x}^*\mathbf{x}}{2} \tag{2}$$

where $\star$ stands for the transpose conjugate and the coefficients of (1) have been stacked into a column vector $\mathbf{x}$. Typically, a smooth radiation pattern is desired for the design of an antenna. Hence, N will be kept low in the range $[2, 5]$.

Then, it is proven in Appendix A that the intensity of the electric field (in W/m^2) at an observation point $\mathbf{r}$, computed from the ray-tracing simulations, can be expressed through the following quadratic form :

$$I(\mathbf{r}) = \mathbf{x}^* \ \mathbf{Q}(\mathbf{r}) \ \mathbf{x} \tag{3}$$

where $\mathbf{Q}$ is a $N \times N$ semi-definite positive matrix. From there, we formulate an optimisation problem for enhancing the coverage of a base station within a certain surrounding built area Ω. Precisely, we want to maximize the field intensity I within Ω while keeping the power P radiated by the antenna constant. This is formulated as

$$\begin{aligned} \min_{\mathbf{x}} \quad & -\mathbf{x}^\star \sum_i \mathbf{Q}(\mathbf{r}_i) \ \mathbf{x} \\ \text{s.t.} \quad & P = \frac{\mathbf{x}^\star\mathbf{x}}{2} \end{aligned} \tag{4}$$

where $\mathbf{r}_i \in \Omega$. In Section VI, the numerical solution of (4) will be obtained with the help of the interior point algorithms implemented in Matlab [17] language.

IV. Parasitic Antenna Array

The objective here is to carry out the beamforming and obtain the objective radiation patterns from the existing base station antennas without replacing them. Therefore, parasitic antennas with different loads are placed in front of the existing base station antenna to form the parasitic array. The set of parasitic loads which form different objective radiation patterns are computed efficiently, which is crucial to the design process of a parasitic array.

A. Driven Antennas of the Parasitic Array

The driven antennas considered here are the base station antennas which are typically used for LTE communication. It consists of 10 crossed dipoles vertically stacked with dual polarization of +45°/-45° [18]. For transmission, the base stations transmit vertically polarized waves by simultaneously exciting the +45°/-45° arms of each crossed dipole. In this paper only the transmission scenario is considered with vertical polarization. The antenna also has a back reflector; it transmits only in a sector of about 64° in a horizontal plane (half power beam-width) and about 6.8° in a vertical plane (half power beam-width). The narrow beam in the vertical plane is achieved through beamforming, using a corporate feeding network implemented with coaxial cables. The design details of the base station antenna itself are not given here for confidentiality reasons. The frequency of operation considered is 1800 MHz, as it is in use for LTE mobile communication. The bandwidth requirement for LTE applications is usually 20 MHz [19].

B. Design of the Parasitic Antennas of the Parasitic Array

The parasitic radiators considered are printed half-wavelength vertical dipoles. Hence, they only impact the directional distribution of fields transmitted by the driven antennas; not their polarization. The parasitic elements themselves need to be essentially resonant to have sufficient impact on the radiation patterns. Moreover, as open radiating structures, their intrinsic bandwidth is not extremely narrow (about 2%) such that that the bandwidth of the parasitic elements is not critically limiting the bandwidth of the whole system.

It has been noticed that, if parasitic dipoles are placed at a distance smaller than a half-wavelength ($\lambda/2$), they disrupt the matching of existing base station antennas. A distance between $\lambda/2$ and λ is appropriate to have a strong mutual coupling between driven (active) and parasitic elements without significantly affecting the matching of the driven elements. Therefore, the parasitic dipoles are placed at a distance λ from the BS antenna, as shown in Fig. 2(a). The parasitic dipoles are placed at a $\lambda/4$ distance from each other, as depicted in Fig. 2(c). In front of each driven crossed dipole of the BS antenna, 12 parasitic dipoles are placed, therefore a total of 12×10 parasitic dipoles and loads are placed in front of the 10 driven elements (BS antenna), as shown in Fig. 2(b). The vertical distance between the rows of parasitic dipoles is 4.55 cm, where each row of 12 parasitic dipoles is aligned in front of each driven element of the base station antenna, as shown in Fig. 2(c). There are three sets of parasitic dipoles, each made of a flat panel containing 4×10 dipoles as shown in Fig. 2(d) which provides a top view of the antenna array. The two panels on left and right sides are tilted at an angle of 30° towards the driven elements (BS antenna) in order to maintain a similar radial distance between all the parasitic dipoles and the driven antennas.

C. Electromagnetic Model for the Simulations

The Electromagnetic model (EM) used for the design of the parasitic array utilizes the open-circuit patterns of all driven and parasitic elements, as well as the array impedance matrix, to include all the mutual coupling information. The embedded element pattern of all the antennas are related to the open-circuit patterns through following equation [4], [20], [21]:

$$\mathbf{f}^e = (\mathbf{Z}^a + \mathbf{Z}^L)^{-1}\mathbf{f}^{O.C.} \tag{5}$$

Here $\mathbf{f}^e$ are the embedded patterns, $\mathbf{f}^{O.C.}$ are the open-circuit patterns, $\mathbf{Z}^L$ is a diagonal matrix containing the load

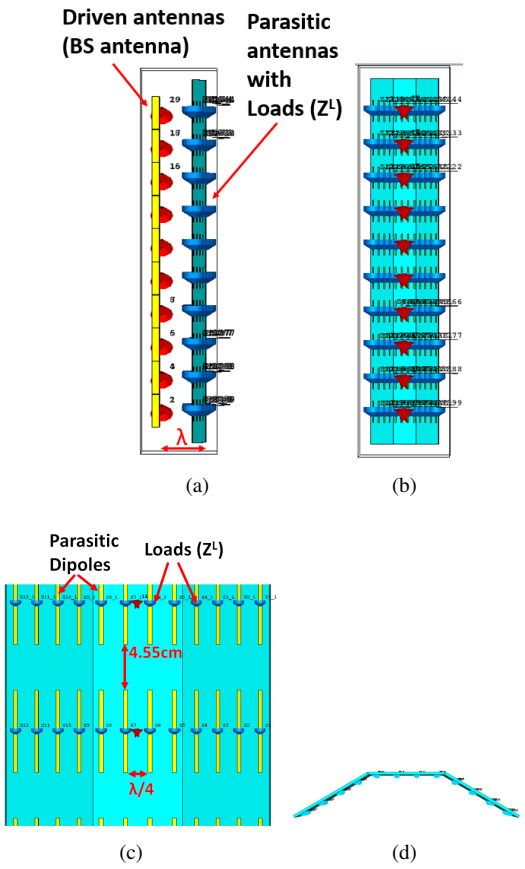

Fig. 2. Parasitic antenna array design for base station: (a) side (b) interior front (c) interior front (zoomed) (d) top.

impedances attached to the driven and parasitic antennas, $\mathbf{Z}^a$ is the N-port impedance matrix containing mutual coupling information. The embedded patterns correspond to patterns obtained with the elements of interest fed with a unit-voltage Thevenin source, while the other elements are passively terminated. The open-circuit patterns suppose a unit-current source at the element of interest, while all other elements are open-circuited. In $\mathbf{f}^e$ and $\mathbf{f}^{O.C.}$ matrices, each row corresponds to a given antenna and each column corresponds to a given direction.

The load values for the driven antennas are usually fixed (50 Ω matched to the RF source), while the loads attached to the parasitic elements can be varied. By varying the entries of the $\mathbf{Z}^L$ matrix the embedded element patterns can be adapted [8]. The total radiation pattern of the array is obtained as the superposition of the embedded patterns of the driven elements only. Hence, beamforming and beam-shaping can be implemented by just varying the loads attached to the parasitic elements. A method-of-moments (MoM) code developed in-house is used for the simulation of the parasitic array. The $\mathbf{Z}^a$ matrix and open-circuit patterns of all the antennas are computed once and saved in memory, as by definition they do not vary with the load terminations. Only the embedded patterns are to be recomputed by superposition according to (5), for different load terminations. It makes this approach computationally efficient for the computation of $\mathbf{Z}^L$, as there is no need to re-simulate the whole array for different load terminations. The parasitic loads are the main dynamic design parameters of a parasitic array which form different radiation patterns.

D. Computation of the Parasitic Loads

The computation (optimization) of loads in a parasitic array is a non-linear problem, which makes it really difficult to efficiently find the set of loads that yields the desired radiation pattern. Therefore the optimization algorithm is crucial to the design of parasitic arrays. The mean-square-error between parasitic array radiation pattern and objective radiation pattern is used as a cost function; it is minimized by varying the loads in order to obtain the radiation pattern with desirable characteristics. The parasitic loads considered are purely imaginary (capacitive or inductive) because the real part of the impedance introduces losses. If $\mathbf{f}(\theta,\phi)$ is an array radiation pattern, $\mathbf{f}_{obj}(\theta,\phi)$ is an objective radiation pattern and $\mathbf{a}(\theta,\phi)$ is a weighting function, then the cost function is defined as:

$$\arg \min_{\bar{Z}_1,..\bar{Z}_N} \int_0^{2\pi}\int_0^{\pi} \mathbf{a}(\theta,\phi)[|\mathbf{f}(\theta,\phi)| - |\mathbf{f}_{obj}(\theta,\phi)|]^2 sin\theta\, d\theta\, d\phi$$

In this paper only azimuthal beamforming is considered, therefore, in every column identical loads are considered. Hence, in the design presented in this paper, there are 12 different parasitic loads in each column of a given row while in one column all 10 rows have the same load. In this paper, the harmonic optimization presented in [9] is used to minimize the cost function efficiently. It considers the loads along a line or a circle, and the load values are decomposed into spatial harmonics according to the positions of the parasitic elements. The optimum load configuration can be expressed as a summation of sines and cosines of different harmonics, as given in (6). For each harmonic, the amplitudes of sines and cosines are optimized, such that the radiation pattern obtained with the sum of harmonics minimizes the cost function. The equations (5) and (6) are used in conjunction to determine (optimize) the parasitic loads $\mathbf{Z}^L$ to obtain different objective radiation patterns.

$$Z^n_{Lmin} = j\sum_{p=1}^{N}(a_p \cos\frac{2\pi np}{N} + b_p \sin\frac{2\pi np}{N}). \qquad (6)$$

Here N is the total number of parasitic loads, p is the harmonic being optimized, n is the element index, a_p and b_p are the purely real amplitudes of cosines and sines, respectively.

E. Simulation Results of the Parasitic Array

The base station antenna [18] shown in Fig. 3(a) is simulated using MoM; the 3D and the 2D radiation patterns at 1800 MHz are shown in Fig. 3(b) and 3(c), respectively. This antenna is used to cover a sector of a base station, it has a back reflector which makes its radiation pattern directive in the azimuth plane. There are multiple antennas stacked vertically inside the casing, which makes it even more directive in the elevation plane.

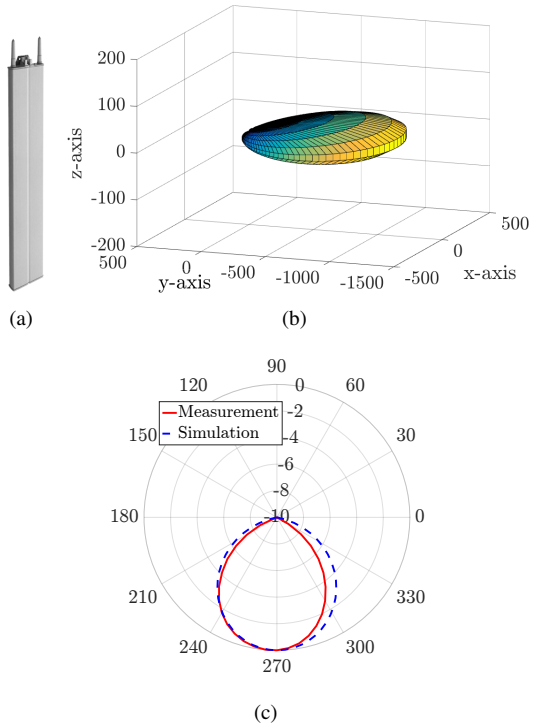

Fig. 3. (a) Base station antenna for a sector in a cellular communication [18] (b) 3D Radiation pattern at 1800 MHz (MoM simulation) (c) azimuthal radiation pattern at 1800 MHz (MoM simulation vs measurement).

The parasitic array consisting of a base station antenna (driven antennas) and printed parasitic dipoles with loads on their terminals is shown in Fig. 4. This array is simulated by using the MoM and the loads values are determined to obtain different objective radiation patterns. The loads values are determined by using EM model in conjunction with the harmonic optimization explained in Section IV-C and Section IV-D, respectively. The simulation results are shown in Fig. 5 and the corresponding optimized loads Z^L are given in Table I. The base station antenna is facing towards $\phi = 270°$, and by changing the loads attached to the parasitic radiators beamforming and beam-shaping is achieved. Case I contains one of the optimized objective patterns obtained through the propagation tools described in Section III. In Case II the objective pattern is synthesized to check the beam-shaping capabilities of the parasitic array. The relative errors between the objective and obtained patterns (simulations) are -10.5 dB and -11.3 dB for Case I and Case II, respectively. The relative errors have been computed using the following relation:

$$Error_{dB} = 10 \cdot log_{10}\left[\frac{\int_0^{2\pi}(|\mathbf{F}_{obj}| - |\mathbf{F}_{obtained}|)^2\, d\phi}{\int_0^{2\pi}|\mathbf{F}_{obj}|^2\, d\phi}\right] \quad (7)$$

In order to scan a beam at wider angles with low SLLs, parasitic elements should surround the driven antenna at wider angles. A rule of thumb we have established through simulations is that a beam can be scanned with low SLLs in the range of $\pm(\alpha - HPBW/2)$, where α is the widest angle at which a parasitic element is placed from broadside and HPBW is the half power beam width of the scanned beam.

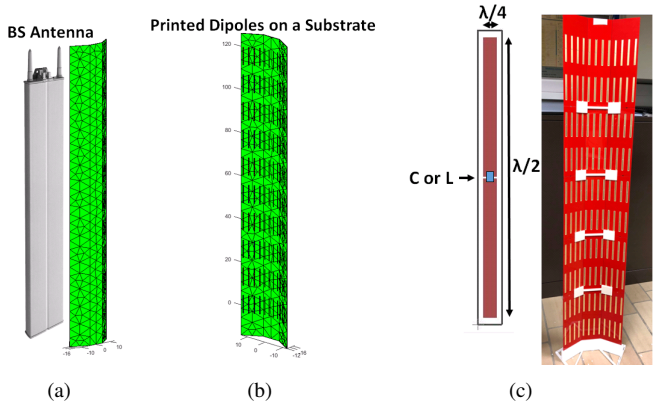

Fig. 4. (a) Base station antenna [18] and printed parasitic dipoles on a substrate with loads (b) interior front of printed parasitic dipoles on a substrate with loads (c) fabricated prototype consisting of printed dipole on I-Tera with capacitors or inductors, the frame is made of AM50C material.

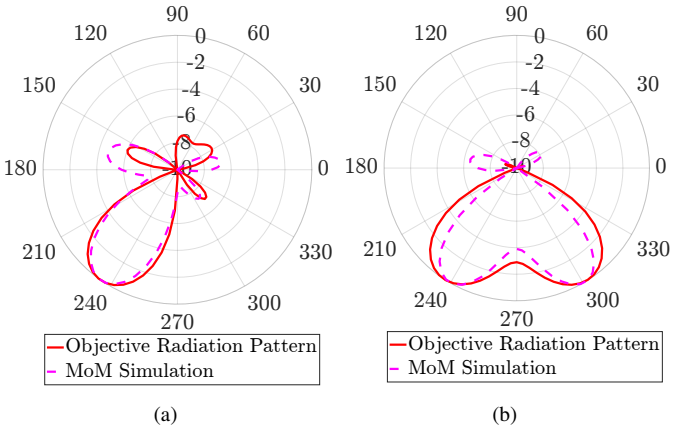

Fig. 5. Different objective radiation patterns and obtained simulated radiation patterns from the parasitic array (a) case I (b) case II.

F. Realization of the Parasitic Radiators with Loads

The parasitic dipoles are printed on I-Tera substrate ($\epsilon_r = 3.38$, $tan\,\delta = 0.002$) [22], the capacitors and inductors computed from the optimized impedances are soldered across the dipole terminals. A frame of material AM50C (ABS/PPMA) ($\epsilon_r = 2.89$, $tan\,\delta = 0.005$) of 3 mm thickness is built and with slots to place the parasitic elements. Then printed dipoles on the I-Tera with capacitors or inductors are placed into the frame as shown in Fig. 4. The frame is placed at a distance λ from the base station antenna to obtain the objective radiation pattern.

Since the fixed capacitors and inductors are placed onto the dipole terminals, only a fixed beam scanning is obtained with this prototype (no electronic scanning). Two different prototypes are fabricated, requiring two different sets of loads,

TABLE I
PARASITIC REACTANCES FOR DIFFERENT RADIATION PATTERNS SHOWN IN FIG. 5

Case I		Case II	
Parasitic Reactance	**Component**	**Parasitic Reactance**	**Component**
308i	27.23nH	-476i	0.1857pF
305i	26.96nH	-352i	0.251pF
292i	25.81nH	-43i	2.075pF
264i	23.34nH	552i	48.79nH
181i	16nH	516i	45.65nH
172i	15.2nH	444i	39.28nH
115i	10.16nH	31i	2.73nH
265i	23.43nH	-251i	0.352pF
159i	14.05nH	-16i	5.46pF
-108i	0.818pF	-136i	0.648pF
-75i	1.17pF	61i	5.38nH
-41i	2.15pF	-331i	0.267pF

to obtain two different radiation patterns from the same base station antenna. In order to achieve the electronic beam scanning, varactors need to be used, which will be explained in Section V. For the proposed parasitic array, 120 varactors will be required which entails the challenge of their biasing. In a given column, the loads are identical, because azimuthal beamforming is considered here. Therefore, if varactors are utilized, all the varactors in a single column will require a common biasing voltage. Moreover, in order to minimize the scattering from biasing lines of varactors, biasing lines can be run through the parasitic dipoles from top to bottom of the array and we will need inductors/chokes to cut RF field.

G. Measurement Results of the Parasitic Array

Radiation pattern of the base station antenna is measured in an anechoic chamber and its comparison with the simulation results is shown in Fig. 3(c). After that, radiation patterns of parasitic array are measured by placing the prototypes in front of the base station antenna. The measured radiation patterns obtained with the two different prototypes are compared with the simulated patterns (MoM and CST [23]) and with the the objective radiation patterns, as shown in Fig. 6. This comparison shows a good agreement between the objective patterns, simulated patterns (MoM) and measured patterns. Slightly higher side-lobe levels in measured patterns can be attributed to inaccuracies in the alignment of parasitic elements with respect to driven elements. The relative errors (7) between the objective patterns and obtained patterns (measurements) are -8.35 dB and -8.56 dB for Case I and Case II, respectively. The radiation patterns are measured across the bandwidth of 20 MHz to cater for LTE applications [19]. The stability of radiation patterns versus frequency can be appreciated in Fig. 7.

One of the issues in the design of parasitic array is the deterioration of the reflection coefficient S_{11} of the driven antenna in the presence of parasitic elements, due to strong

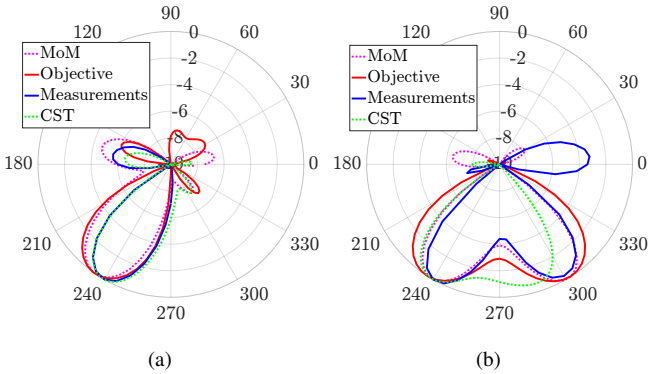

Fig. 6. Comparison of objective radiation pattern, simulations (MoM, CST) and measurements (a) case I (b) case II.

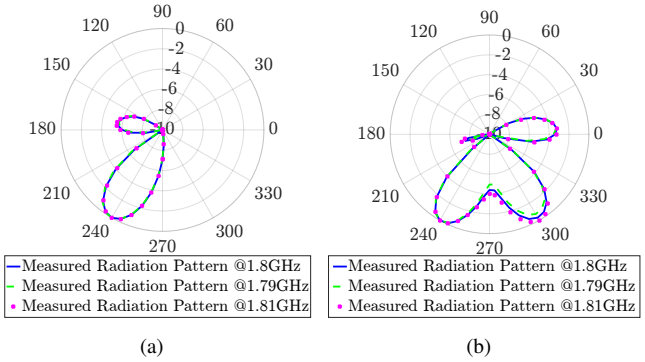

Fig. 7. Variation of radiation patterns versus frequency (a) case I (b) case II.

mutual coupling. Here, since the parasitic elements are placed at a one-wavelength distance, the deterioration of the reflection coefficient of a base station antenna is not significant, and S_{11} is still under -10 dB from 1.6 GHz to 2.5 GHz. Fig. 8 gives the comparison of the measured reflection coefficient of the base station antenna with and without the parasitic elements (two prototypes). The radiation efficiency computed from CST simulation is 98.9% because of use of low loss substrate (we consider this estimate obtained with CST as quite optimistic).

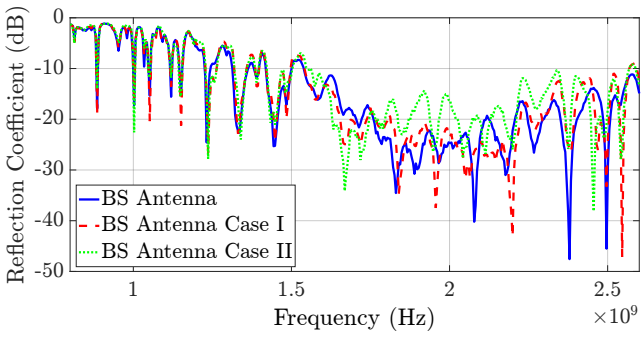

Fig. 8. Measured reflection coefficient of BS antenna: isolated and with two different parasitic arrays.

V. Electronically Steerable Parasitic Array Radiator (ESPAR) Antenna

A. Design of the ESPAR Antenna

In order to steer the beam electronically in a parasitic array, an impedance is needed that can be varied electronically. Therefore, a varactor diode is used here in reverse biased condition; its capacitance varies by changing the DC bias voltage. The MAVR-011020-1411 diode [24] is used because of its suitable range of capacitance $(0.19\,pF - 0.025\,pF)$. Its data sheet gives the range of capacitance with respect to variable DC bias at 1 MHz. For our application it needs to be characterized at 1800 MHz to find out the exact impedance provided by it at the terminals of the parasitic elements. Since a varactor diode gives only a variable capacitive impedance, a fixed inductor is placed in series with the varactor diode in order cover both positive and negative reactances. Large inductors are placed in series with DC feed to block the RF currents flowing on the DC bias lines, in order to minimize the scattering from the DC bias lines. Although the DC bias lines are made very thin and RF chokes are used to minimize the scattering, they are still included in the EM simulation and the load optimization procedure, to take into account for the residual scattering.

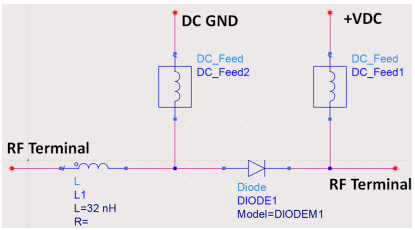

Fig. 9. Schematics of variable impedance circuit of varactor in series with inductor (ADS).

The characterization of the circuit shown in Fig. 9 has been carried out at 1800 MHz. Fig. 10 shows the measured impedance with respect to the DC bias. It can be seen that by changing the DC bias, both capacitive and inductive impedance can be obtained.

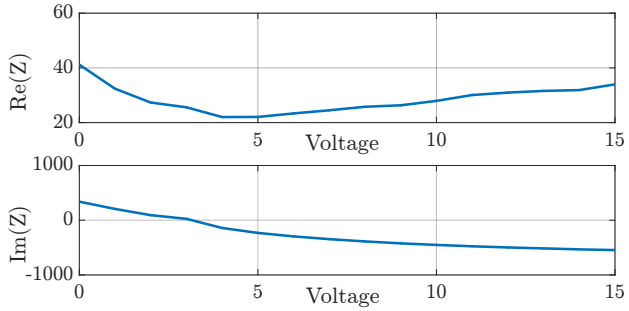

Fig. 10. Measured impedance of the circuit at 1800 MHz.

A prototype has been designed following the same methodology explained in Section IV-C and Section IV-D, to obtain the different objective radiation patterns. However, in this case, the variable-impedance circuit is used to show that the different radiation patterns can be obtained electronically. This prototype has been designed for a single driven element of the base station antenna to keep it simple, although the same design methodology can be used for the whole base station antenna. A single antenna element has been designed for base station application [25]. The fabricated test antenna can be seen in Fig. 11(a), its simulated and measured patterns are shown in Fig. 12.

A prototype, consisting of four printed parasitic dipoles is designed with the characterized variable impedance circuit placed at the terminals of the dipoles. The half-wavelength (8.3 cm) parasitic dipoles of width $\lambda/40$ (0.4 cm) are printed on the I-Tera substrate with DC bias lines of 0.1 mm thickness, which are used to tune the impedance of the circuit. The parasitic loads computed to obtain the desired patterns, are given in Table II. Digital-to-analog converters controlled by computer are utilized to vary the DC bias voltages. The fabricated prototype is shown in Fig. 11.

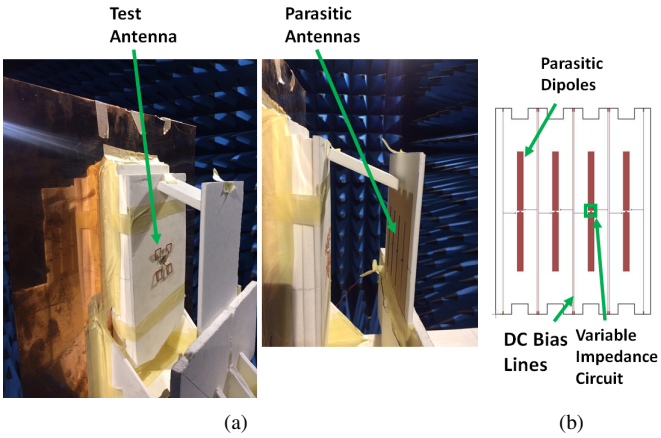

Fig. 11. (a) Fabricated ESPAR antenna (b) parasitic radiators with biasing circuitry.

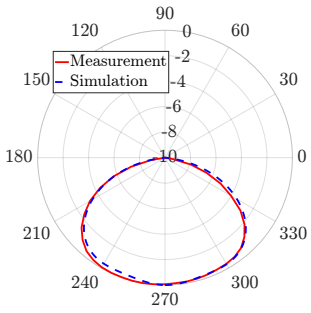

Fig. 12. Radiation pattern of test antenna at 1800 MHz (simulation vs measurement).

B. Measurements of the ESPAR Antenna

The fabricated prototype is tested in an anechoic chamber to verify its beam scanning capabilities. The comparison between objective radiation patterns, simulated patterns and measured patterns is shown in Fig. 13. The two straight dotted lines in each plot delineate the widest angle $\pm\alpha$ at which the parasitic

element is placed from broadside. The antenna is oriented towards an angle of 270°, by just changing the DC bias voltages the main beam can be steered in either directions. The relative errors (7) between the objective and obtained patterns (simulations) are -7.05 dB and -5.83 dB for Case I and Case II, respectively. The obtained radiation patterns in simulations have higher side lobes as compared to the prototype with fixed loads described in Section IV. The reason is that fewer parasitic radiators are used to modulate the radiation pattern and hence they do not truly surround the driven antenna. This limited number of controllable loads prevented scanning the beam at wider angles while maintain low SLLs. The results shown in Fig. 13 depict a good agreement between the simulation and experimental results, except for slightly higher SLLs in the measured patterns as compared to the simulation results. The relative errors between the objective and obtained patterns (measurements) are -2.82 dB and -4.42 dB for Case I and Case II, respectively. The relative error is large in measurements, for the smaller prototype. The discrepancy in the measured patterns can be attributed to inaccuracies in the alignment of parasitic elements with respect to the driven element.

The characteristics of varactors may vary from one sample to another and also with the ageing and temperature. Calibration of varactors, as inserted in the array, can be carried out to delineate the varactor's characteristics through a comparison between the modulated pattern and its observed value in a number of directions. To this end machine-learning techniques [26], [27] may help to reduce the number of experiments.

It has been shown that the objective radiation patterns obtained from propagation studies, can be achieved from a base station antenna using a parasitic array. Now the far fields obtained with the designed parasitic array are simulated again using propagation tools in order to verify the RF power level in a cell.

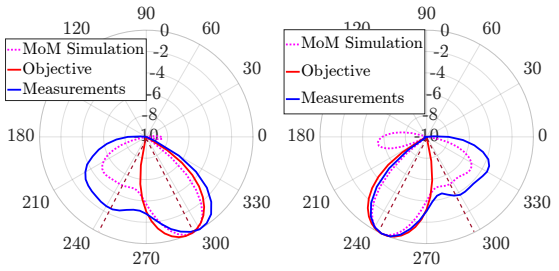

Fig. 13. Simulation and experimental results of ESPAR antenna (a) case I (b) case II.

VI. Improved Coverage Results with Optimized Base-Station

In this section, we will compare the level of the electric field (in dBμV/m), in a realistic built environment, computed from in-house ray-tracing simulations using the pattern of the initial base station antenna (without parasitic elements) and the modulated patterns (with parasitic array). A top view of the simulated area, as well as the position and orientation of two base stations (BS) are shown in Fig. 14. The antennas and the observation points lie in a horizontal plane at 2 m above the ground.

TABLE II
Parasitic reactances and DC biases for different radiation patterns of ESPAR prototype shown in Fig. 13

Case I		Case II	
Parasitic Reactance	**DC Bias**	**Parasitic Reactance**	**DC Bias**
62i	2.5V	-253i	5.6V
-292i	6V	-536i	14V
51i	2.6V	-315i	6.4V
-282i	5.9V	137i	1.6V

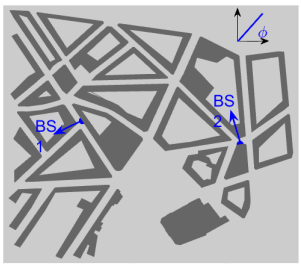

Fig. 14. Top view of the geometry of the scenario with buildings (grey) and two base stations (blue dots-arrows).

The relative permittivity and the conductivity of the concrete walls and ground are set to $\epsilon_r = 4.44$ and $\sigma = 0.01$, respectively [28]. The expansion order N of the objective pattern (1) is set to 3 and the radiated power per antenna is 0.1 W. Only contributions from line-of-sight and first-order reflections are considered in the ray-tracing simulations. The field level obtained with the initial BS pattern (without parasitic elements) and with the modulated patterns (with the parasitic array) are illustrated in Fig. 15. One can see that, across the simulated area, for the same radiated power, the field level obtained with the BS with the parasitic array is slightly higher than that when using only BS pattern. The reason of improvement is that the parasitic array has shaped and rotated the radiation patterns of two BSs, in order to better illuminate the nearest surrounding street as compared to the initial BS antenna pattern, as shown in Fig. 16.

Finally, a comparison is made in Fig. 17 between the Cumulative Distribution Functions (CDFs) of the field levels obtained with the initial pattern and the modulated radiation patterns (MoM simulations) for both BSs. This confirms the improvement of the radio coverage since the CDFs associated to the modulated patterns are shifted to the right of the CDF of the initial BS pattern by approximately 3-4 dB.

VII. Conclusion

A parasitic array has been designed and tested in the laboratory to implement beamforming and beam-shaping for 4G

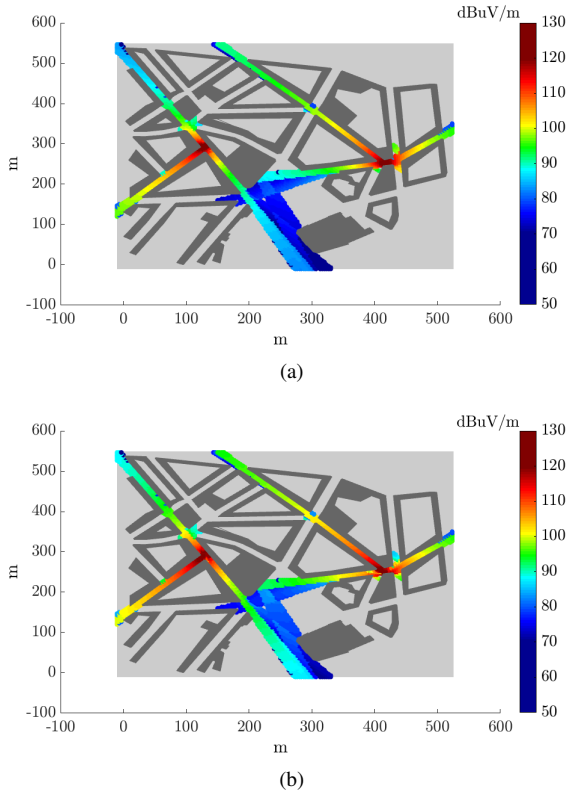

Fig. 15. Ray-tracing simulation of the amplitude of the electrical field in dBμV/m with the (a) BS patterns (b) modulated BS patterns with parasitic array.

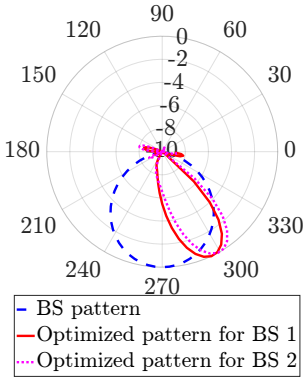

Fig. 16. BS pattern vs modulated BS patterns with parasitic array.

and 5G communication base station antennas. It is shown that such beamforming and beams-shaping can also be employed to modulate the RF power exposure level in a given area. The overall problem has been split in two parts: a propagation-oriented optimization problem which uses ray-tracing simulations to produce objective patterns that enhance the field coverage while respecting a prescribed tolerance of field levels over a given area, and a design-oriented optimization problem which finds the loads of parasitic dipoles to modulate the pattern of a base station antenna such that it is as close as possible to the objective pattern. The EM model and the harmonic optimization technique utilized in this paper can be efficiently combined for the design of parasitic arrays.

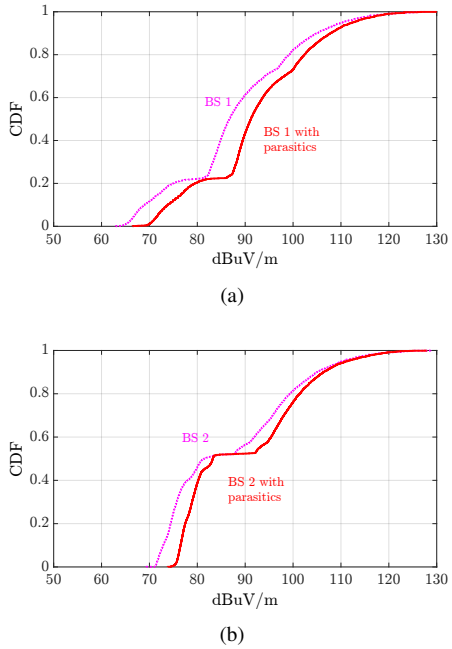

Fig. 17. CDF of the field level from BS antenna and from BS antenna with parasitic array for (a) BS 1 (b) BS 2.

Varactor diodes are used as variable impedances to steer the beam electronically, as demonstrated with a smaller array. Ray-tracing simulations have been performed for a realistic scenario and they highlight an improvement in the coverage because of the modulated radiation patterns of base station comprising of the parasitic antenna array. The simulation and experimental results for designed parasitic antenna array prototypes are also in a good agreement.

APPENDIX

FIELD INTENSITY FROM RAY-TRACING SIMULATIONS

A ray-tracing simulation leads classically [29] to the following representation of the electric field at an observation point $\mathbf{r}$:

$$\mathbf{E}(\mathbf{r}) = \sum_{l=1}^{L(\mathbf{r})} \mathbf{D}_l(\mathbf{r})\ \mathbf{f}(\theta_l, \phi_l) \tag{8}$$

where $L(\mathbf{r})$ is the number of rays propagating from the antenna to the observation point, (θ_l, ϕ_l) are the departure angles of ray l from the antenna and $\mathbf{D}_l$ is a 3×3 matrix that accounts for electromagnetic interactions with the geometry of the buildings. Then, by inserting (1) into (8), the field intensity (in W/m^2) associated to each ray is expressed through a quadratic form as:

$$I_l(\mathbf{r}) = \mathbf{x}^*\ \mathbf{Q}_l(\mathbf{r})\ \mathbf{x} \tag{9}$$

where $\mathbf{Q}_l$ is a $N \times N$ matrix and its element ij is given by:

$$Q_l^{ij}(\mathbf{r}) = \frac{1}{2\eta}\ \mathbf{f}_i^\star(\theta_l, \phi_l)\ \mathbf{D}_l^*(\mathbf{r})\ \mathbf{D}_l(\mathbf{r})\ \mathbf{f}_j(\theta_l, \phi_l) \tag{10}$$

where η is the free-space impedance. Knowing that the phase of each ray field cannot be predicted due to the inaccuracy of

the geometrical modelling of the buildings, it is reasonable to assume that rays reaching an observation point $\mathbf{r}$ are uncorrelated. Hence, in the mean sense, the total intensity is given by the sum of that of each rays:

$$\mathbf{Q}(\mathbf{r}) = \sum_{l} \mathbf{Q}_l(\mathbf{r}) \tag{11}$$

ACKNOWLEDGEMENT

We would like to acknowledge SIRRIS (Ir. Didier Garray) for their contribution in providing the material and design for the frame supporting parasitic elements.

REFERENCES

[1] A. Ahlbom, U. Bergqvist, J. Bernhardt, J. Cesarini, M. Grandolfo, M. Hietanen, A. Mckinlay, M. Repacholi, D. H. Sliney, J. A. Stolwijk *et al.*, "Guidelines for limiting exposure to time-varying electric, magnetic, and electromagnetic fields (up to 300 GHz)," *Health physics*, vol. 74, no. 4, pp. 494–521, 1998.

[2] Z. Zaharis, "Radiation pattern shaping of a mobile base station antenna array using a particle swarm optimization based technique," *Electrical Engineering*, vol. 90, no. 4, pp. 301–311, 2008.

[3] V. Degli-Esposti, G. Riva, and N. Binucci, "Derivation of antenna pattern shaping criteria for urban base stations using ray tracing," *IEEE Trans. Vehicular Techn.*, vol. 52, no. 6, pp. 1686–1688, Nov. 2003.

[4] R. Harrington, "Reactively controlled directive arrays," *IEEE Trans. Antennas Propaga.*, vol. 26, no. 3, pp. 390–395, May. 1978.

[5] A. Kausar, H. Mehrpouyan, M. Sellathurai, R. Qian, and S. Kausar, "Energy efficient switched parasitic array antenna for 5G networks and IoT," in *Loughborough Antennas Propaga. Conf. (LAPC)*, pp. 1–5, Nov. 2016.

[6] T. Ohira and K. Iigusa, "Electronically steerable parasitic array radiator antenna," *Electronics and Comm. in Japan (Part II: Electronics)*, vol. 87, no. 10, pp. 25–45, 2004.

[7] Z. Li, E. Ahmed, A. M. Eltawil, and B. A. Cetiner, "A beam-steering reconfigurable antenna for WLAN applications," *IEEE Trans. Antennas Propaga.*, vol. 63, no. 1, pp. 24–32, Jan. 2015.

[8] J. Aelterman, R. Goossens, F. Declercq, and H. Rogier, "Ant colony optimisation-based radiation pattern manipulation algorithm for electronically steerable array radiator antennas," *IET Sci. Meas. Tech.*, vol. 3, no. 4, pp. 302–311, Jul. 2009.

[9] H. A. Kayani, K. Alkhalifeh, and C. Craeye, "Open-circuit to embedded pattern approach with harmonic optimization in ESPAR," in *IEEE MTT-S Int. Conf. Num. Electromag. Multiphys. Model. Optim. RF, Microw. Terah. App. (NEMO)*, pp. 31–33, May. 2017.

[10] D. Rodrigo and L. Jofre, "Frequency and radiation pattern reconfigurability of a multi-size pixel antenna," *IEEE Trans. Antennas Propaga.*, vol. 60, no. 5, pp. 2219–2225, May. 2012.

[11] M. Ohira, A. Miura, M. Taromaru, and M. Ueba, "Efficient gain optimization techniques for azimuth beam/null steering of inverted-F multiport parasitic array radiator (MuPAR) antenna," *IEEE Trans. Antennas Propaga.*, vol. 60, no. 3, pp. 1352–1361, Mar. 2012.

[12] L. Ge, X. Yang, Z. Dong, D. Zhang, and X. Zeng, "Reconfigurable magneto-electric dipole antennas for base stations in modern wireless communication systems," *Wireless Comm. Mobile Comput.*, 2018.

[13] A. Edalati and T. A. Denidni, "High-gain reconfigurable sectoral antenna using an active cylindrical FSS structure," *IEEE Trans. Antennas Propaga.*, vol. 59, no. 7, pp. 2464–2472, Jul. 2011.

[14] M. Bouslama, M. Traii, T. A. Denidni, and A. Gharsallah, "Beam-switching antenna with a new reconfigurable frequency selective surface," *IEEE Antennas Wireless Propag. Lett.*, vol. 15, pp. 1159–1162, 2016.

[15] J. Y. Lau and S. V. Hum, "Reconfigurable transmitarray design approaches for beamforming applications," *IEEE Trans. Antennas Propaga.*, vol. 60, no. 12, pp. 5679–5689, Dec. 2012.

[16] J. Hansen, *Spherical near-field antenna measurements*. London, U.K.: P. Peregrinus on behalf of the Institution of Electrical Engineers, 1988.

[17] "MATLAB 2014a, The MathWorks, Natick." [Online]. Available: https://mathworks.com/products/matlab.html

[18] KATHREIN Antennen Electronics, "2-multi-band F-panel dual polarization half-power beam width adjust. electr. downtilt," 2017, Data Sheet. [Online]. Available: https://www.kuenten.com/joescms/images/content/dokumente/Bundesgericht/B4-Datenblatt-K-742236.pdf

[19] M. Nohrborg, "LTE." [Online]. Available: http://www.3gpp.org/technologies/keywords-acronyms/98-lte

[20] D. F. Kelley, "Relationships between active element patterns and mutual impedance matrices in phased array antennas," in *IEEE Antennas Propag. Soci. Int. Symp.*, vol. 1, pp. 524–527, Jun. 2002.

[21] C. Craeye and D. Gonzalez-Ovejero, "A review on array mutual coupling analysis," *Radio Science*, vol. 46, no. 2, pp. 1–25, Apr. 2011.

[22] isola, "I-Tera MT RF very low-loss laminate material," 2018, Data Sheet. [Online]. Available: https://www.isola-group.com/wp-content/uploads/data-sheets/i-tera-mt40-rfmw.pdf

[23] "CST studio suite 2017, CST-computer simulation technology AG." [Online]. Available: https://www.cst.com/solutions/markets/antennas

[24] MACOM, "Solderable GaAs constant gamma flip-chip varactor diode MAVR-011020-1411," 2017, Data Sheet. [Online]. Available: http://cdn.macom.com/datasheets/mavr-011020-1141.pdf

[25] G. Cui, S.-G. Zhou, G. Zhao, and S.-X. Gong, "A compact dual-band dual-polarized antenna for base station application," *Progress In Electromagne. Rese.*, vol. 64, pp. 61–70, May. 2016.

[26] C. Huang, G. C. Alexandropoulos, A. Zappone, C. Yuen, and M. Debbah, "Deep learning for UL/DL channel calibration in generic massive MIMO systems," *arXiv preprint arXiv:1903.02875*, 2019.

[27] H. Peng, Z. Yang, and T. Yang, "Design and implementation of a practical direction finding receiver," *Progress In Electromagne. Research Letters*, vol. 32, pp. 157–167, 2012.

[28] Y. Miao, Q. Gueuning, and C. Oestges, "Modeling the phase correlation of effective diffuse scattering from surfaces for radio propagation prediction with antennas at refined separation," *IEEE Trans. Antennas Propaga.*, vol. 66, no. 3, pp. 1427–1435, Mar. 2018.

[29] M. F. Catedra, J. Perez, F. S. de Adana, and O. Gutierrez, "Efficient ray-tracing techniques for three-dimensional analyses of propagation in mobile communications: application to picocell and microcell scenarios," *IEEE Antennas Propag. Mag.*, vol. 40, no. 2, pp. 15–28, Apr. 1998.

Husnain Ali Kayani was born in Jhelum, Pakistan, in 1989. He received his BE in electrical engineering from National University of Sciences and Technology (NUST), Islamabad, Pakistan, in 2011. He received his MS in electrical engineering from Université catholique de Louvain (UCL), Louvain-la-Neuve, Belgium and Polytechnic University of Turin (PdT), Italy, in 2015. He had worked as "Core Network Engineer" in Mobilink Pakistan from 2011 to 2013. Currently he is pursuing his PhD at UCL in electrical engineering and working on Electronically Steerable Parasitic Array Radiators (ESPARs) for the base station antennas of 5G communication systems.

He had won scholarship from NUST throughout his BE from 2007 to 2011. He was a recipient of Erasmus Mundus Scholarship from European Union for a double degree MS program from 2013 to 2015.

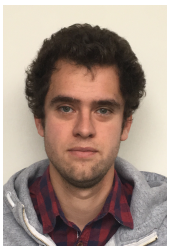

Quentin Gueuning received the M.Sc. and the Ph.D. degrees in electrical engineering from the Université catholique de Louvain (UCL), Louvain-la-Neuve, Belgium in 2014 and 2019, respectively. Currently, he is working as a Research Associate at the Cavendish Laboratory, University of Cambridge, UK. His main research interests include EM computational methods and theories applied to radio-channel characterization and radio astronomy.

Nicolas Goreux received the M.Sc. degree in mechatronics engineering from the Université catholique de Louvain (UCL), Louvain-la-Neuve, Belgium in 2017. He has worked as a research assistant at UCL from 2017 to 2018. Currently, he is working at IBA, Louvain-la-Neuve, Belgium.

Danielle Vanhoenacker-Janvier (M'88–SM'90) received the M.S. degree in electrical engineering and the Ph.D. degree in Applied Sciences from the Université catholique de Louvain (UCL), Louvain-la-Neuve, Belgium, in 1978 and 1987, respectively.

Since 2000, she has been a Professor with UCLouvain, where she has been a Full Professor since 2007. She was the Head of the Microwave Laboratory, Louvain-la-Neuve, from 2001 to 2006 and in charge of Student Affairs at the Louvain School of Engineering, Louvain-la-Neuve, from 2001 to 2011. She has been the Chair of the Doctoral Commission since 2015. Her main activity domain is the study and modeling of atmospheric effects on propagation of radio waves above 10 GHz for more than 30 years, with a special interest in the propagation through turbulent troposphere and in the use of Numerical Weather Prediction software for the simulation of atmospheric effects. New applications are foreseen at optical wavelengths. Her group is also involved in the simulation of the radar cross section of airplanes wake vortices and the evaluation of the Doppler spectrum. She is also active in microwave circuit design. She has authored more than 120 technical papers. She is the coauthor of one book.

Dr. Vanhoenacker-Janvier is a reviewer for various international conferences and IEEE and IEE journals. She has acted as an expert for the evaluation of research teams in various countries. She is the Secretary General of the European Microwave Association.

Claude Oestges (F'16) received the M.Sc. and Ph.D. degrees in electrical engineering from the Université catholique de Louvain (UCL), Louvain-la-Neuve, Belgium, in 1996 and 2000, respectively. In 2001, he joined the Smart Antennas Research Group (Information Systems Laboratory), Stanford University, Stanford, CA, USA, as a Post-Doctoral Scholar. From 2002 to 2005, he was with the Microwave Laboratory, UCL, as a Post-Doctoral Fellow of the Belgian Fonds de la Recherche Scientifique (FRS-FNRS). He is currently a Full Professor with the Electrical Engineering Department, Institute for Information and Communication Technologies, Electronics and Applied Mathematics, UCL. He has authored or co-authored over three books and more than 200 journal papers and conference communications. Dr. Oestges has been the Chair of COST Action CA15104 IRACON since 2016. He was a recipient of the 1999-2000 IET Marconi Premium Award and the IEEE Vehicular Technology Society Neal Shepherd Award in 2004 and 2012.

Christophe Craeye (M'98–SM'11) was born in Ronse, Belgium in 1971. He received the Electrical Engineering and Bachelor in Philosophy degrees and the Ph.D. degree in applied sciences from the Université catholique de Louvain (UCL), Louvain-la-Neuve, Belgium, in 1994 and 1998, respectively. From 1994 to 1999, he was a Teaching Assistant with UCL and carried out research on the radar signature of the sea surface perturbed by rain, in collaboration with NASA and ESA. From 1999 to 2001, he was a Postdoctoral Researcher with the Eindhoven University of Technology, Eindhoven, The Netherlands. His research there was related to wideband phased arrays devoted to the square kilometer array radio telescope. In this framework, he was also with the University of Massachusetts, Amherst, MA, USA, in the Fall of 1999, and was with the Netherlands Institute for Research in Astronomy, Dwingeloo, The Netherlands, in 2001. In 2002, he started an antenna research activity at the Université catholique de Louvain, where he is now a Professor. He was with the Astrophysics and Detectors Group, University of Cambridge, Cambridge, U.K., from January to August 2011. His research is funded by Région Wallonne, European Commission, ESA, FNRS, and UCL. His research interests include finite antenna arrays, wideband antennas, small antennas, metamaterials, and numerical methods for fields in periodic media, with applications to communication and sensing systems.

Prof. Craeye served as an Associate Editor for the *IEEE transactions on antennas and propagation* and for the *IEEE Antennas and Wireless Propagation Letters* from 2011 to 2017. In 2009, he was the recipient of the 2005-2008 Georges Vanderlinden Prize from the Belgian Royal Academy of Sciences.